Room temperature ballistic transport in InSb quantum well nanodevices

A. M. Gilbertson, A. Kormányos, P. D. Buckle, M. Fearn, T. Ashley, C. J. Lambert, S. A. Solin, and L. F. Cohen

Citation: Applied Physics Letters **99**, 242101 (2011); doi: 10.1063/1.3668107
View online: http://dx.doi.org/10.1063/1.3668107
View Table of Contents: http://scitation.aip.org/content/aip/journal/apl/99/24?ver=pdfcov
Published by the AIP Publishing

Room temperature ballistic transport in InSb quantum well nanodevices

A. M. Gilbertson,[1,a)] A. Kormányos,[2] P. D. Buckle,[3] M. Fearn,[2] T. Ashley,[4] C. J. Lambert,[2] S. A. Solin,[1,5] and L. F. Cohen[1]
[1]*Blackett Laboratory, Imperial College, London SW7 2BZ, United Kingdom*
[2]*Department of Physics, Lancaster University, Lancaster LA1 4YB, United Kingdom*
[3]*Department of Physics and Astronomy, Cardiff University, Cardiff CF24 CAA, United Kingdom*
[4]*School of Engineering, University of Warwick, Coventry CV4 7AL, United Kingdom*
[5]*Center for Materials Innovations and Department of Physics, Washington University in St. Louis, Missouri-63130, USA*

(Received 7 October 2011; accepted 18 November 2011; published online 12 December 2011)

We report the room temperature observation of significant ballistic electron transport in shallow etched four-terminal mesoscopic devices fabricated on an InSb/AlInSb quantum well (QW) heterostructure with a crucial partitioned growth-buffer scheme. Ballistic electron transport is evidenced by a negative bend resistance signature which is quite clearly observed at 295 K and at current densities in excess of 10^6 A/cm^2. This demonstrates unequivocally that by using effective growth and processing strategies, room temperature ballistic effects can be exploited in InSb/AlInSb QWs at practical device dimensions. © *2011 American Institute of Physics*. [doi:10.1063/1.3668107]

Harnessing ballistic transport effects in low-dimensional structures at room temperature (RT) is a promising avenue for developing innovative nanoelectronic devices for applications including logic circuits, biosensing, and high-density data storage. Carbon-based systems such as carbon nanotubes (CNTs)[1,2] and graphene[3] have received considerable attention owing to their extraordinarily long mean free path (l_0) at RT (<50 μm in CNTs) and high current carrying capability, but the realization of very-large-scale-integration compatibility remains a fundamental challenge. In this respect, high mobility III-V semiconductors are technologically relevant. Several groups[4,5] have explored ballistic switching and rectifying concepts in InGaAs/InP quantum wells (QWs), where $l_0 \approx 150$ nm at 295 K. The operating efficiency of such devices is closely linked to the ratio of l_0 to the critical device dimension and is limited to ~20% due to the small value of l_0 in such systems. Electron mobilities of $\mu_e \approx 45\,000$ cm^2/Vs are routinely achieved in InSb/AlInSb QWs at 295 K—the largest reported of any III-V system.[6] For a typical electron density $n_e \approx 6 \times 10^{11}$ cm^{-2}, this corresponds to $l_0 = \hbar k_F \mu_e / e \approx 550$ nm (where $k_F = (2\pi n_e)^{1/2}$). Considerable advantages would be afforded by pursuing such device concepts in this system; however, to-date, the RT operation of InSb QW nanodevices has been inhibited by excessive buffer layer leakage currents.[7]

In this letter, we report the magnetotransport properties of mesoscopic devices fabricated on an InSb/AlInSb QW with a partitioned buffer layer (PBL) scheme[8] designed to suppress the parasitic leakage currents, which demonstrate remarkably clear ballistic transport at 295 K as a result.

The sample used is a 15-nm modulation doped InSb/$Al_xIn_{1-x}Sb$ QW grown by MBE onto a GaAs (001) substrate with a PBL scheme (growth details are found elsewhere[8]). A 15-nm pseudomorphic $Al_{0.3}In_{0.7}Sb$ layer is incorporated 300 nm below the QW to provide a potential barrier to electrons and holes, thermally generated in the bulk of the buffer layer, from diffusing to the ohmic contact region. In this way, the effective electrical thickness of the buffer layer is reduced from 3 μm to 300 nm. The electron density and mobility of the QW at 295 K are $n_e = 7.31 \times 10^{11}$ cm^{-2} and $\mu_e = 41\,500$ cm^2/Vs ($l_0 = 586$ nm), as deduced from high magnetic field measurements on 40-μm-wide (reference) Hall bridges.[8] Mesoscopic cross structures of various sizes were fabricated using *e*-beam and optical lithography and shallow (100 nm etch depth) reactive ion etching (RIE) in a CH_4/H_2 (1:8) gas mixture. Magnetotransport measurements were performed in perpendicular magnetic fields (B) up to 7.5 T at various temperatures using standard AC and DC measurement techniques. The sidewall depletion width, w_{dep}, was estimated from the dependence of the two-terminal conductance (G_{2T}) (B = 0) of several devices on the physical lead width at 160 K to be $w_{dep} \approx 120$ nm (not shown).

We have investigated ballistic electron transport at elevated temperatures by studying the bend resistance $R_B = (V_4 - V_3)/I_{21}$ (see Fig. 1 insets). If at B = 0, a large proportion of electrons injected from lead 1 are ballistic, those with large forward momentum are transmitted directly to the opposite lead 3. This raises the potential of lead 3 with respect to lead 4, generating a negative bend resistance (NBR). A small magnetic field deflects the electron beam away from lead 3 into one of the side leads causing the NBR to decay. The resulting dip in R_B(B) (centered on B = 0) is a clear signature of ballistic transport. The NBR anomaly has previously not been observed above 200 K in InSb/AlInSb devices.[7]

The results for R_B(B) obtained from a symmetric cross with physical lead width $w_0 = 550$ nm (*S*550) and an asymmetric cross width w_0 (w_1) = 360 (660) nm (*A*360) between 160 K and 295 K are shown in Figs. 1(a) and 1(b), respectively (device geometries are shown in the insets). At 160 K, a distinct NBR is observed in both devices with an amplitude and full width at half maximum (FWHM) that remains approximately constant up to 240 K. Remarkably, the NBR feature persists up to 295 K indicating significant ballistic

a)Electronic mail: a.gilbertson@imperial.ac.uk.

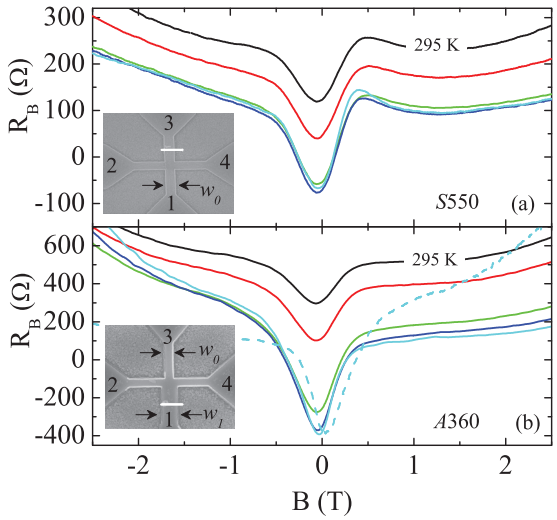

FIG. 1. (Color online) (a) and (b) Bend resistance $R_B(B) = (V_4 - V_3)/I_{21}$ measurements at various temperatures between 160 K and 295 K for two different device geometries. From top to bottom, T = 295 K, 280 K, 240 K, 200 K, and 160 K. The dashed line in (b) represents the reciprocal measurement $R^{\dagger}_B(B)$ at 160 K. Insets show electron micrographs of the devices. An AC current of 100 nA was used.

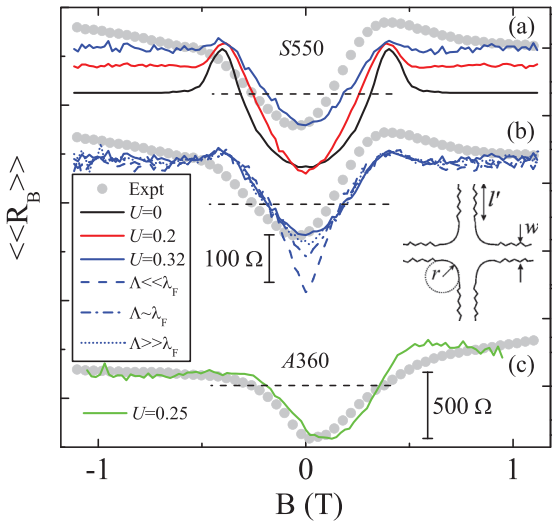

FIG. 2. (Color online) Quantum calculations of the energy-impurity averaged bend resistance $\ll R_B(B) \gg$ (lines) with varying disorders compared to the experimental data at 160 K (symbols). (a) *S*550 with smooth sidewalls and impurity potential as labeled. (b) S550 with $U = 0.32$ and sidewall roughness as labeled. (c) *A*360 with $U = 0.25$ and smooth sidewalls. Fluctuations are due to interference effects that are not fully averaged out. Horizontal dashed lines indicate $R_B = 0$. (A corner rounding radius $r = 120$ nm and lead length $l' = 1.7$ μm was used in all cases, see inset.)

electron transport in the QW. This result demonstrates that the parasitic effects of parallel conduction in the buffer layer have been substantially suppressed by wafer design, and moreover, that the processing strategy has not degraded μ_e to the point that all carriers are diffusive as is reported in InAs/AlSb devices.[9] The NBR feature is superposed on a background resistance (R_{bg}) that is approximately constant (≈100 Ω) below 240 K and rises with increasing temperature such that $R_B(0)$ is no longer negative. Nevertheless, ballistic coupling of leads 1 and 3 is evident by the persistent dip at B = 0. This background will be discussed further in comparison to theoretical modeling. A secondary feature of the bend resistance data is the asymmetry of the magnetic field response. The geometrical origin of this is confirmed by measurements of the resistance $R^{\dagger}_B = (V_1 - V_2)/I_{34}$ which satisfies very closely the reciprocity relation $R_B(B) = R^{\dagger}_B(-B)$, as shown for device *A*360 by the dashed line in Fig. 1(b).

Measurements of the Hall resistance, $R_H = (V_4 - V_2)/I_{31}$, were also performed. The electron densities of the mesoscopic devices (n_{mes}) were estimated from the Hall slope, at fields (≈0.5 T) where ballistic anomalies are absent, to be $n_{mes} = 5\ (3.75) \times 10^{11}\ \mathrm{cm}^{-2}$ and $n_{mes} = 4.5\ (3.5) \times 10^{11}\ \mathrm{cm}^{-2}$ at 295 K (160 K), for *S*550 and *A*360, respectively.

To gain further insight into the microscopic properties of the devices, we have performed extensive numerical quantum transport calculations of $R_B(B)$ using a tight-binding code which combines the Green's function techniques of Baranger *et al.*[10] and Sanvito *et al.*[11] Some effects of finite temperature were simulated using a simple energy-averaging technique that takes into account the Fermi distribution.[10] We consider two possible types of disorder in the devices: elastic scattering from impurities and from the sidewalls (shown to be important in our previous work).[12] Impurity scattering was modeled with Anderson site-disorder; the on-site energies of the tight-binding Hamiltonian were chosen from an interval $[-U,U]$ with uniform probability.[10] Sidewall scattering was taken into account by introducing a boundary roughness characterized by a mean amplitude (Δ) and correlation length (Λ) after Akera *et al.*[13] We use $\Delta = 5$ nm (deduced from atomic force microscopy of the lateral etched surface) and consider the three limits: $\Lambda \ll \lambda_F$, $\Lambda \sim \lambda_F$, and $\Lambda \gg \lambda_F$, where $\lambda_F = 2\pi/k_F$ is the Fermi wavelength. Electron-phonon scattering is not included in this simple model; however, as we will show, the impurity scattering model captures the essential features of momentum scattering within the channel.

Figures 2(a) and 2(b) shows the energy-impurity averaged bend resistance curves (lines), $\ll R_B(B) \gg$, for device *S*550 with varying disorder compared to the experimental data at 160 K (symbols). Note that we have used the experimental n_{mes} and the effective electrical lead widths w_{eff} ($w_{eff} = w - 2w_{dep}$). In the absence of disorder $\ll R_B(B) \gg$ has zero background resistance, and an NBR that is both broader and larger in amplitude ($\ll \Delta R_B \gg$) than observed experimentally. Finite R_{bg} is, therefore, clear evidence of disorder in the experimental devices. The quantum calculations provide confirmation that the observed low-field (<1 T) characteristics of $R_B(B)$ are determined almost entirely by scattering in the channel rather than by scattering at the boundaries: (1) Calculations with only sidewall scattering yield $\ll \Delta R_B \gg$ up to 10 times greater than the experimental data due to enhanced electron collimation[14] (not shown for clarity); (2) R_{bg} is sensitive to the strength of impurity scattering [Fig. 2(a)] but is relatively insensitive to the presence, or type, of boundary roughness [Fig. 2(b)]; and (3) A comparison of $\ll \Delta R_B \gg$ with and without surface roughness [Fig. 2(b)] to experiment suggests little enhancement from diffuse collimation in the present devices. Indeed, good agreement with the experimental data is found for the $\ll R_B(B) \gg$ curves with smooth boundaries ($\Delta = 0$) and $U = 0.32$ (solid line Fig. 2(b)). Similar results were found for device *A*360 [Fig. 2(c)]. Note that the assumption of smooth

sidewalls is consistent with large w_{dep} due to electrostatic screening of the exterior sidewall roughness.

The effective channel mobility (μ_{eff}) for a given disorder can be obtained from calculations of G_{2T} for single leads of varying length (l') in diffusive limit where the relation $G_{2T}(l') = n_{mes} e \mu_{eff} (w/l')$ is valid. The disorder corresponding to the solid curves in Figs. 2(b) and 2(c), yield $\mu_{eff} \approx 45\,000$ cm^2/Vs. Comparing this value obtained from 0 K quantum calculations to that of the reference sample at 160 K, we find ≈30% reduction in the former case, suggesting that some degradation has occurred due to the nanofabrication process.

We now discuss the operation of our devices in the high bias, nonequilibrium transport regime relevant for nanoelectronic applications where large signals are required. In principle, hot-ballistic electron transport is limited by LO phonon emission ($\hbar\omega_0 = 25$ meV in InSb), but at 295 K the thermal broadening of the electron distribution is already rather large (≈ 26 meV), and thus, hot electron effects should be less acute.

The forward bias *IV* characteristic of device *A*360 ($w_{0eff} \sim 130$ nm) at 295 K is shown in Fig. 3(a). A distinct nonlinearity is observed at high bias current, but note that the differential resistance is positive over the entire range due to the diffuse background. Figure 3(b) shows the nonmonotonic dependence of the DC NBR amplitude ΔR_B on I_{21}. Synonymous with the above is a broadening of the NBR with increasing I_{12} [see inset to Fig. 3(a)]. Since the FWHM (B_{FWHM}) is proportional to k, the broadening is a direct indication of the excess kinetic energy ($\Delta E \approx eV_{34}$) gained in the nonequilibrium regime where $k \propto k_F(1 + \Delta E/E_F)^{1/2}$ and E_F is the Fermi energy.[15] Likewise, if we assume $\Delta R_B(\Delta E,T) \propto \exp[-w_{0eff}/v_F(1 + \Delta E/E_F)^{1/2}\tau(\Delta E,T)]$,[16] where v_F and $\tau(\Delta E,T)$ are the Fermi velocity and momentum-scattering time, respectively, the behavior for $I_{21} < 25\ \mu$A can be understood by an increasing electron velocity, and $\tau(\Delta E)$ that is essentially energy independent for $\Delta E < \hbar\omega_0$. The turnover occurs at a voltage $eV_{34} \approx \hbar\omega_0$ [see Fig. 3(a)], at which point injected electrons have sufficient energy to scatter by phonon emission, and $\tau(\Delta E,T)$ is reduced substantially. This is consistent with the theory of optical phonon scattering, but contrary to previous reports at low temperature,[15,16] the observed hot electron effects are considerably less acute and demonstrate that RT ballistic effects persist *without decay* up to $eV_{34} \approx \hbar\omega_0$.

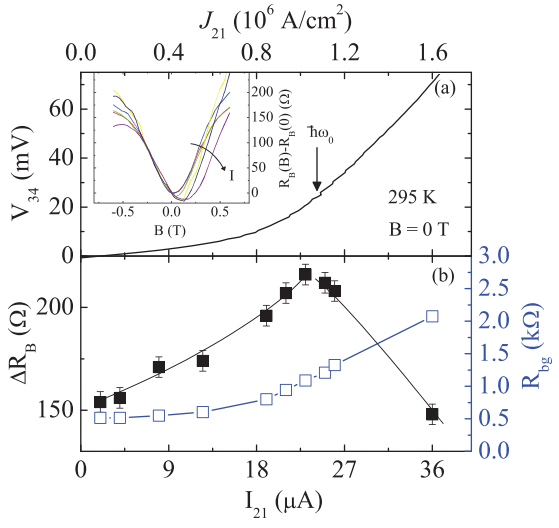

FIG. 3. (Color online) (a) *IV* characteristic of device *A*360 ($w_{0eff} = 130$ nm) at B = 0 T and 295 K. Inset: The DC bend resistance $R_B(B)$–$R_B(0)$ at various currents illustrating the effect of broadening. (b) The dependence of the DC $\Delta R_b(B)$ (solid symbols) and R_{bg} (open symbols) on bias current. $\Delta R_B(I_{21})$ exhibits a turnover at $I_{21} \approx 25\ \mu$A ($eV_{43} \approx \hbar\omega_0$) due to LO phonon emission that lowers l_0.

Finally, we can consider these devices as examples of quasi-ballistic Hall probes. The magnetic sensitivity is given by the noise-equivalent-field (NEF) $B_{NEF} = V_n/I_{31}R'$, where V_n is the voltage noise and R′ the Hall coefficient (Ω/T). For device *A*360, we have $R_{2T} = 20$ kΩ and $R' = 1390$ Ω/T at 295 K, giving $B_{NEF} \approx 500$ nT/$\sqrt{\text{Hz}}$ for a bias current of 25 μA (where we have used the Johnson noise limit $V_n^2 = 4k_BTR_{2T}$). This sensitivity is considerably greater than the previous reports of sub-micron Hall probes[9,17] and magnetoresistance sensors at RT,[18,19] demonstrating that although not yet optimized, the ballistic cross structures we report here are highly competitive and hold significant promise for future high resolution RT sensors.

This work was supported by the UK EPSRC under Grant No. EP/F065922/1. S.A.S. is also supported by the U.S. NSF under Grant No. ECCS-0725538 and NIH under Grant No. 1U54CA11934201, and has a financial interest in PixelEXX, a start-up company whose mission is to market imaging arrays.

[1]A. Javey, J. Guo, Q. Wang, M. Lundstrom, and H. Dai, Nature **424**, 654 (2003).
[2]S. Frank, P. Poncharal, Z. L. Wang, and W. A. d. Heer, Science **280**, 1744 (1998).
[3]A. S. Mayorov, R. V. Gorbachev, S. V. Morozov, L. Britnell, R. Jalil, L. A. Pnomarenko, P. Blake, K. S. Novoselov, K. Watanabe, T. Taniguchi *et al.*, Nano Lett. **11**, 2396 (2011).
[4]K. Hieke and M. Ulfward, Phys. Rev. B **62**, 16727 (2000).
[5]A. M. Song, P. Omling, L. Samuelson, W. Seifert, I. Shorubalko, and H. Zirath, Appl. Phys. Lett. **79**, 1357 (2001).
[6]J. M. S. Orr, A. M. Gilbertson, M. Fearn, O. W. Croad, C. J. Storey, L. Buckle, M. T. Emeny, P. D. Buckle, and T. Ashley, Phys. Rev. B **77**, 165334 (2008).
[7]N. Goel, S. J. Chung, M. B. Santos, K. Suzuki, S. Miyashita, and Y. Hirayama, Physica E **20**, 251 (2004).
[8]A. M. Gilbertson, P. D. Buckle, M. T. Emeny, T. Ashley, and L. F. Cohen, Phys. Rev. B **84**, 075474 (2011).
[9]L. Folks, A. S. Troup, T. D. Boone, J. A. Katine, M. Nishioka, M. Grobis, G. G. Sullivan, A. Ikhassi, M. Field, and B. A. Gurney, J. Phys. C **21**, 255802 (2009).
[10]H. U. Baranger, D. P. DiVincenzo, R. A. Jalabert, and A. D. Stone, Phys. Rev. B **44**, 10637 (1991).
[11]S. Sanvito, C. J. Lambert, J. H. Jefferson, and A. M. Bratkovsky, Phys. Rev. B **59**, 11936 (1999).
[12]A. M. Gilbertson, M. Fearn, A. Kormanyos, D. E. Read, C. J. Lambert, M. T. Emeny, T. Ashley, S. A. Solin, and L. F. Cohen, Phys. Rev. B **83**, 075304 (2011).
[13]H. Akera and T. Ando, Phys. Rev. B **43**, 11676 (1991).
[14]R. J. Blaikie, K. Nakazato, J. R. A. Cleaver, and H. Ahmed, Phys. Rev. B **46**, 9796 (1992).
[15]J. G. Williamson, H. van Houten, C. W. J. Beenakker, M. E. I. Broekaart, L. I. A. Spendeler, B. J. van Wees, and C. T. Foxon, Phys. Rev. B **41**, 1207 (1990).
[16]T. Schäpers, G. J. Kruger, J. Appenzeller, A. Forster, B. Lengeler, and H. Luth, Appl. Phys. Lett. **66**, 3603 (1995).
[17]O. Kazakova, V. Panchal, J. Gallop, P. See, D. C. Cox, M. Spasova, and L. F. Cohen, J. Appl. Phys. **107**, 09E708 (2010).
[18]S. A. Solin, D. R. Hines, A. C. H. Rowe, J. S. Tsai, Y. A. Pashkin, S. J. Chung, N. Goel, and M. B. Santos, Appl. Phys. Lett. **80**, 4012 (2002).
[19]T. D. Boone, N. Smith, L. Folks, J. A. Katine, E. E. Marinero, and B. A. Gurney, IEEE Electron Device Lett. **30**, 117 (2009).